ARCHIVES OF ELECTRICAL ENGINEERING VOL. 68(4), pp. 817–830 (2019)

DOI 10.24425/aee.2019.130685

Analysis of fault states in drive systems with multi-phase induction motors

JACEK JAN LISTWAN

Wroclaw University of Science and Technology
Department of Electrical Machines, Drives and Measurements
Wybrzeze Wyspianskiego 27, 50-370 Wroclaw, Poland
e-mail: jacek.listwan@pwr.edu.pl

(Received: 13.02.2019, revised: 12.06.2019)

Abstract: The paper presents the analysis of different fault states in drive systems with multi-phase induction motors. The mathematical models of a five-phase and six-phase induction motor and the MRAS^{CC} estimator have been presented and the description of the Space Vector Modulation has been shown. The Direct Field-Oriented Control (DFOC) system is analyzed. Results of the simulation and experimental studies of the Direct Field-Oriented Control systems in the fault conditions are presented. The author's original contribution includes analysis and studies of the DFOC control method of a five-phase induction motor resistant to the motor speed sensor fault with the use of the MRAS^{CC} estimator.

Key words: Direct Field-Oriented Control method, Fault Tolerant Control, MRAS^{CC} estimator, multi-phase squirrel-cage induction motor, sensorless drives, Voltage Source Inverter faults

1. Introduction

Development of frequency converters provides the possibility of applications of induction motors with the number of stator phases greater than three. The interest in the multi-phase induction motors is caused by the reduction of the power per phase in comparison with the three-phase induction motors, reducing the ripples of the electromagnetic torque, reducing the losses caused by current higher harmonics in the DC link of the frequency converter and improved reliability [1, 2, 5–10, 12–14]. The motors with the number of stator phases greater than three are usually used in high power applications.

Nowadays the reliability of the drive systems is very important in industry and for this reason, the fault tolerant control methods of the drive systems are developed [3, 4, 13, 14]. The higher reliability of the drive systems can be achieved, for example, by the application of multi-phase

induction motors and by the use of the estimators of motor control variables. The multi-phase induction motors may be conditionally operated upon the failure of one or more stator phases. In the drive systems, the motor speed sensor can be often damaged and in this case, the motor speed signal should be replaced by the signal from a speed estimator.

This article presents the analysis of a five-phase and six-phase induction motor with Direct Field-Oriented Control (DFOC) [6, 8, 11] during the occurrence of different fault states in drive systems. For the drive system with a five-phase induction motor the encoder failure in the control system has been analyzed. For the drive system with a six-phase induction motor, the failure introduced by blocking of the control signals of a three-phase Voltage Source Inverter (VSI), consisting of the part of the six-phase VSI has been analyzed. In the DFOC system with a five-phase induction motor, the MRAS^{CC} estimator of the magnitude of the rotor flux vector and of the motor speed has been used. The conventional estimator of the magnitude of the rotor flux vector, based on the current motor model [11] has been used in the DFOC system with a six-phase induction motor. It is assumed, that other controllers in the DFOC system are the PI controllers for both considered types of multi-phase induction motors.

The simulation and experimental studies of the DFOC systems with multi-phase induction motors have been carried out and the obtained results have been presented and discussed.

2. Mathematical model of multi-phase induction motor

The mathematical models of five-phase and six-phase squirrel-cage induction motors have been formulated on the basis of commonly used simplifying assumptions: a multi-phase stator and rotor windings are considered as concentrated, a motor magnetic circuit is linear, the effects of eddy currents and iron losses are neglected, the values of parameters and variables of the rotor winding are converted to the side of a stator winding [1, 2, 5–10, 12–14]. The analysis and control of these types of motors in the stator and rotor phase coordinate system is quite difficult, because the motor models are then described by the differential equations with the time dependent coefficients. For this reason, the appropriate transformation of phase variables are used and the models of multi-phase induction motors with constant coefficients are obtained. After applying the transformation matrix [12]:

$$[C] = \frac{2}{n} \cdot \begin{bmatrix} 1 & \cos\alpha & \cos 2\alpha & \cos 3\alpha & \cos 4\alpha & \cos 5\alpha \\ 0 & \sin\alpha & \sin 2\alpha & \sin 3\alpha & \sin 4\alpha & \sin 5\alpha \\ 1 & \cos 2\alpha & \cos 4\alpha & \cos 6\alpha & \cos 8\alpha & \cos 10\alpha \\ 0 & \sin 2\alpha & \sin 4\alpha & \sin 6\alpha & \sin 8\alpha & \sin 10\alpha \\ 1/\sqrt{2} & 1/\sqrt{2} & 1/\sqrt{2} & 1/\sqrt{2} & 1/\sqrt{2} & 1/\sqrt{2} \\ 1/\sqrt{2} & -1/\sqrt{2} & 1/\sqrt{2} & -1/\sqrt{2} & 1/\sqrt{2} & -1/\sqrt{2} \end{bmatrix}, \tag{1}$$

($\alpha = 2\pi/n$ is the electrical angle between the axes of the machine phase windings, n is the number of the stator phases) to the stator and rotor equations, the original multi-phase system can be decomposed into several decoupled systems: the stationary α–β coordinate system, the additional coordinate system $z1$–$z2$ and the system of zero components (one zero component

for a five-phase induction motor and two zero components for a six-phase induction motor). The components in the $\alpha-\beta$ coordinate system can be transformed afterwards to the $x-y$ coordinate system, which rotates at arbitrary angular speed ω_k [1, 2, 5–10, 12–14] after applying the transformation matrix presented below:

$$[D_s] = [D_s(\vartheta_k)] = \begin{bmatrix} \cos\vartheta_k & \sin\vartheta_k & & & \\ -\sin\vartheta_k & \cos\vartheta_k & & & \\ & & 1 & & \\ & & & \cdots & \\ & & & & 1 \end{bmatrix}, \tag{2}$$

where: $\vartheta_k = \int_0^t \omega_k \, \mathrm{d}t$; ω_k is the arbitrary angular speed of the coordinate system relative to the stator.

The common general equations for the five-phase and six-phase induction motor after suitable transformations take the following form [1, 2, 5–10, 12–14]:

– the voltage equations for the stator and rotor circuits, expressed in the rectangular $x-y$ coordinate system, which rotates relative to the stator at arbitrary angular speed ω_k:

$$u_{sx} = R_s \, i_{sx} - \omega_k \psi_{sy} + p\psi_{sx}, \tag{3}$$

$$u_{sy} = R_s \, i_{sy} + \omega_k \psi_{sx} + p\psi_{sy}, \tag{4}$$

$$0 = R_r \, i_{rx} - (\omega_k - \omega_e)\psi_{ry} + p\psi_{rx}, \tag{5}$$

$$0 = R_r \, i_{ry} + (\omega_k - \omega_e)\psi_{rx} + p\psi_{ry}, \tag{6}$$

– the stator voltage equations, expressed in the additional coordinate system $z1-z2$:

$$u_{sz1} = R_s \, i_{sz1} + p\psi_{sz1}, \tag{7}$$

$$u_{sz2} = R_s \, i_{sz2} + p\psi_{sz2}, \tag{8}$$

– the equation of the motor electromagnetic torque:

$$T_e = \frac{n}{2} \cdot p_b \cdot \frac{L_m}{L_r} \cdot \left(\psi_{rx} i_{sy} - \psi_{ry} i_{sx}\right), \tag{9}$$

where: u_{sx}, u_{sy}, u_{sz1}, u_{sz2} represent the components of the stator voltage vectors; i_{sx}, i_{sy}, i_{sz1}, i_{sz2}, i_{rx}, i_{ry} are the components of the stator and rotor current vectors; ψ_{sx}, ψ_{sy}, ψ_{sz1}, ψ_{sz2}, ψ_{rx}, ψ_{ry} are the components of the stator and rotor flux linkage vectors; ω_k is the arbitrary angular speed of the coordinate system relative to the stator; ω_e is the electrical angular speed of the rotor; T_e is the motor electromagnetic torque; R_s, R_r represent the stator and rotor phase resistance; L_m is the motor magnetizing inductance; L_r is the rotor inductance; n is the number of stator phase windings; p_b is the number of motor pole pairs; $p = \mathrm{d}/\mathrm{d}t$ is the derivative operator.

The variables considered in the coordinate system $z1-z2$ are not involved in the generation of the electromagnetic torque, but they should be considered in the analysis, because they can cause enlargement of the amplitude of the stator phase currents and power losses in the stator windings. The zero components can be neglected in further analysis because in typical designs of multi-phase induction motors with the phase winding connections in star, these components are always equal to zero.

3. Space vector modulation method

In the research presented in this article it was assumed, that the considered multi-phase induction motors are supplied respectively by a two-level five-phase or six-phase Voltage Source Inverter (VSI). The voltage space vectors generated by the five-phase VSI and by six-phase VSI, expressed in the stationary system $\alpha-\beta$, are presented, respectively, in Figure 1(a) and in Figure 1(b).

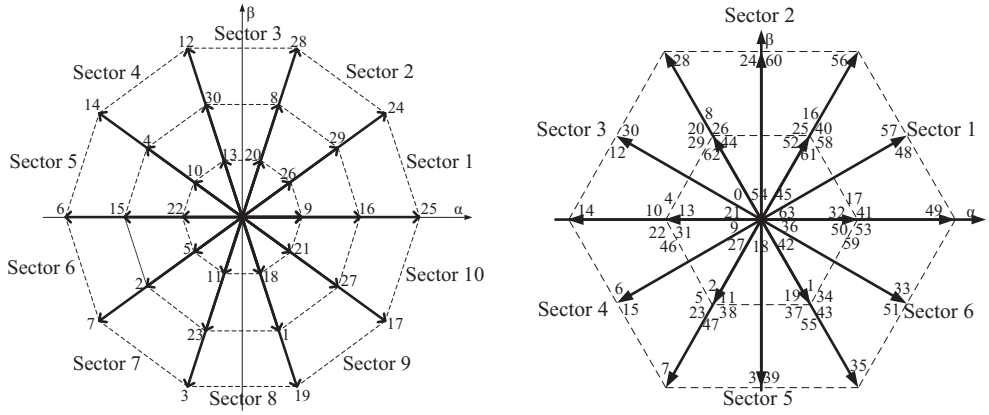

Fig. 1. Voltage space vectors generated in $\alpha-\beta$ coordinate system: (a) by five-phase VSI; (b) by six-phase VSI

The methods of Space Vector Modulation for the five-phase and six-phase VSIs have been based on the synthesis of the reference voltage vector by using the switching times of two long voltage vectors from the same sector in which the reference voltage vector is located and by using the switching times of two zero voltage vectors [1, 2, 5, 10].

As an example, the graphical interpretation of the applied SVM method for a five-phase VSI has been presented in the Figure 2. For the case, when the reference voltage vector $\underline{u}_{s\ \mathrm{ref}}$ falls into Sector 1 it can be synthesized by choosing two long voltage vectors: $\underline{u}_{25}$, $\underline{u}_{24}$ and by suitable choosing two zero voltage vectors $\underline{u}_0$ and $\underline{u}_{31}$.

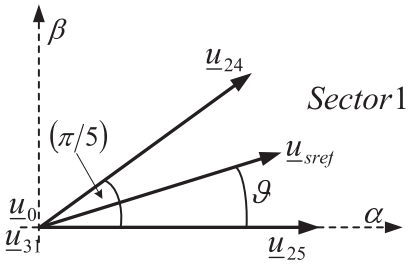

Fig. 2. The principle of space vector modulation for five-phase VSI

For the case presented in Figure 2, when the reference voltage vector is situated in Sector 1, the principle of a space vector modulation method can be described by the following equations:

$$\underline{u}_{s\,\mathrm{ref}} \cdot T_s = \underline{u}_{25} \cdot t_1 + \underline{u}_{24} \cdot t_2 + \underline{u}_0 \cdot \frac{t_0}{2} + \underline{u}_{31} \cdot \frac{t_0}{2}, \tag{10}$$

$$t_0 = T_s - t_1 - t_2, \tag{11}$$

where: t_1, t_2 are the switching times of long voltage vectors; t_0 is the switching time of zero voltage vectors; T_s is the switching period; ϑ is the angle position of the reference stator voltage vector.

4. MRAS^{CC} estimator model

The MRAS^{CC} estimator [3, 4, 9] has been developed for the control systems with three-phase induction motors. In this article MRAS control principles will be generalized to the control system with a multi-phase induction motor. This estimator has been used to the reproduction of the speed signal of the five-phase induction motor and the rotor flux vector in the DFOC control system with the five-phase induction motor, resistant to the damage of the motor speed sensor. It is an adaptive estimator in which the implemented reference model is the model of the induction motor. The block scheme of the MRAS^{CC} estimator is presented in Figure 3 [3, 4, 9].

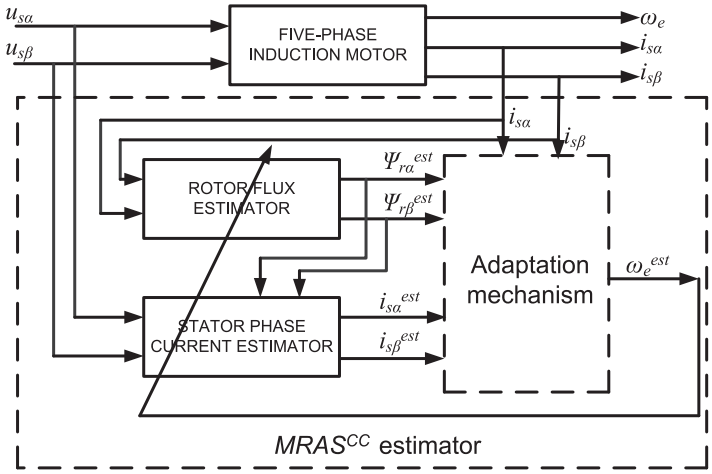

Fig. 3. The block scheme of the MRAS^{CC} estimator

The stator phase currents of the five-phase induction motor are measured and the components of the stator current vector in the $\alpha-\beta$ coordinate system are afterwards determined. These components are compared to the components reproduced by using the stator current-voltage model of the motor [3, 4, 9, 11]. The rotor flux vector estimator [11] is tuned by the angular speed signal of the rotor of the induction motor, determined by the adaptation algorithm. The estimator

of the stator current vector can be obtained with using the voltage model and the current model of the rotor flux estimator [3, 4, 9, 11]. The operation of the estimator of the stator current vector depends on the values: components of a stator voltage vector, components of a rotor flux vector and the rotor angular speed.

The rotor-flux model of the motor is described by the following equations [3, 4, 9, 11]:

$$\begin{aligned} \frac{\mathrm{d}}{\mathrm{d}t}\psi_{r\alpha}^{est} &= \frac{R_r}{L_r}\left(L_m i_{s\alpha}^{est} - \psi_{r\alpha}^{est}\right) - \omega_e^{est}\psi_{r\beta}^{est} \\ \frac{\mathrm{d}}{\mathrm{d}t}\psi_{r\beta}^{est} &= \frac{R_r}{L_r}\left(L_m i_{s\beta}^{est} - \psi_{r\beta}^{est}\right) + \omega_e^{est}\psi_{r\alpha}^{est} \end{aligned}. \tag{12}$$

The stator-current model of the motor is described by the following equations [3, 4, 9, 11]:

$$\begin{aligned} \frac{\mathrm{d}i_{s\alpha}^{est}}{\mathrm{d}t} &= -i_{s\alpha}^{est}\frac{R_r L_m^2 + L_r^2 R_s}{\sigma L_s L_r^2} + \frac{L_m R_r}{\sigma L_s L_r^2}\psi_{r\alpha}^{est} + \frac{L_m}{\sigma L_s L_r}\omega_e^{est}\psi_{r\beta}^{est} + \frac{1}{\sigma L_s}u_{s\alpha} \\ \frac{\mathrm{d}i_{s\beta}^{est}}{\mathrm{d}t} &= -i_{s\beta}^{est}\frac{R_r L_m^2 + L_r^2 R_s}{\sigma L_s L_r^2} + \frac{L_m R_r}{\sigma L_s L_r^2}\psi_{r\beta}^{est} - \frac{L_m}{\sigma L_s L_r}\omega_e^{est}\psi_{r\alpha}^{est} + \frac{1}{\sigma L_s}u_{s\beta} \end{aligned}, \tag{13}$$

where: $i_{s\alpha}^{est}$, $i_{s\beta}^{est}$ are the estimated values of the components of the stator phase current vector in the $\alpha-\beta$ coordinate system; L_s is the stator inductance; $\sigma = 1 - L_m^2/L_s L_r$ is the total leakage factor; $\psi_{r\alpha}^{est}$, $\psi_{r\beta}^{est}$ are the estimated values of the components of the rotor flux vector in the $\alpha-\beta$ coordinate system; ω_e^{est} is the estimated value of the angular electrical motor speed.

The errors between the estimated stator current values and the measured values are used in the motor speed reproduction algorithm, which can be defined as follows [3, 4, 9]:

$$\omega_e^{est} = K_p \cdot \left(e_{i_{s\alpha}} \cdot \psi_{r\beta} - e_{i_{s\beta}} \cdot \psi_{r\alpha}\right) + \frac{1}{T_i}\int \left(e_{i_{s\alpha}} \cdot \psi_{r\beta} - e_{i_{s\beta}} \cdot \psi_{r\alpha}\right) \mathrm{d}t, \tag{14}$$

where: $e_{i_{s\alpha}} = i_{s\alpha} - i_{s\alpha}^{est}$, $e_{i_{s\beta}} = i_{s\beta} - i_{s\beta}^{est}$ represent the errors between the measured and estimated values of the components of the stator current vector in the $\alpha-\beta$ coordinate system; K_p, T_i are the coefficients of the proportional and integral parts of the PI controller.

5. Direct field-oriented control systems

In this article the two faults states have been analyzed for chosen two types of the multi-phase induction motors and for the two different DFOC systems [8, 11].

As Fault State 1, the operation of the DFOC with a six-phase induction motor during occurrence of the fault state consisting in blocking the control of the three-phase Voltage Source Inverter, constituting the component part of the six-phase Voltage Source Inverter was analyzed. As a consequence of this emergency condition, only three phases of the stator windings of the six-phase induction motor are supplied.

As Fault State 2, the damage of the speed sensor of the five-phase induction motor with the DFOC system and MRAS^{CC} estimator [3, 4] was analyzed.

The block diagram of the DFOC system with a five-phase induction motor is shown in Figure 4 and with a six-phase induction motor is shown in Figure 5. In order to implement the DFOC control system of the multi-phase induction motor, the estimator of the instantaneous magnitude and the angle of the rotor flux vector must be used. In the fault tolerant control drives also the motor speed estimator must be applied. The estimator of the magnitude of the rotor flux vector based on the current model of the motor [11] has been used in the DFOC system with a six-phase induction motor and the MRAS^{CC} estimator of the magnitude of the rotor flux vector and the motor speed has been used in the DFOC system with a five-phase induction motor.

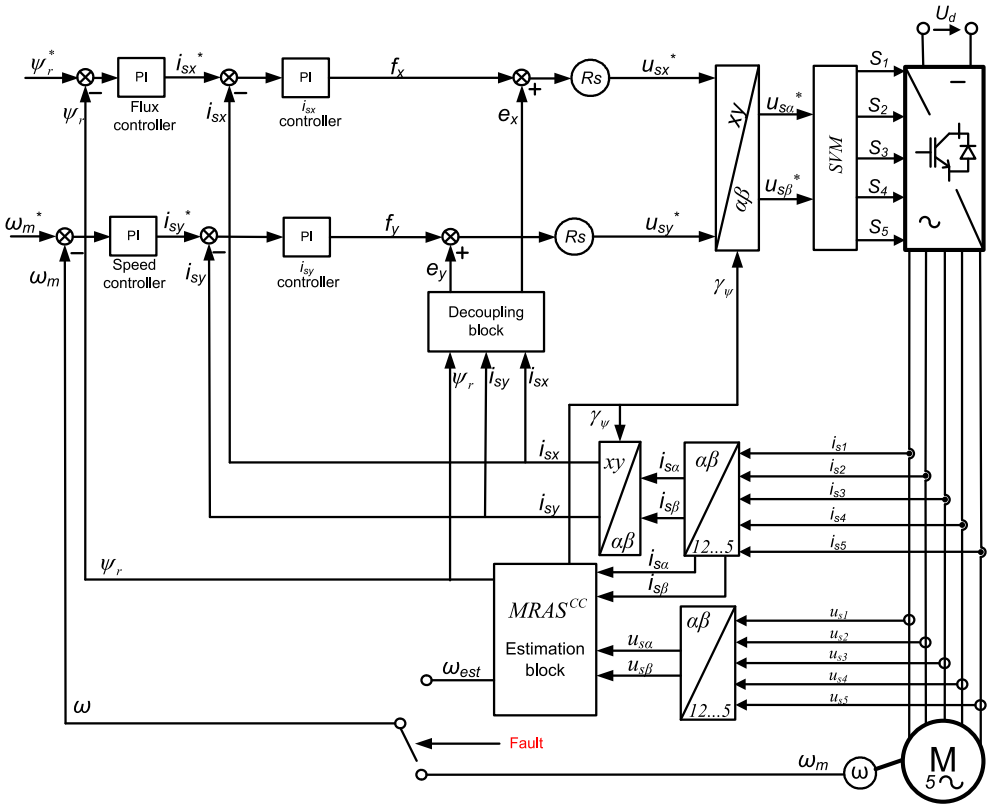

Fig. 4. The control system of five-phase induction motor with Direct Field-Oriented Control and MRAS estimator

The DFOC control schemes for analyzed multi-phase induction motors consist of four control loops. The first outer control loop regulates the motor mechanical speed ω_m and the second outer control loop regulates the magnitude of the rotor flux vector ψ_r. The x component of the stator current vector, responsible for the rotor flux control is determined by the PI controller of magnitude of the rotor flux vector and the y component of the stator current vector, responsible for electromagnetic torque control is determined by the PI speed controller. The both inner control loops with PI controllers regulate values of the x and y components of the stator current vector.

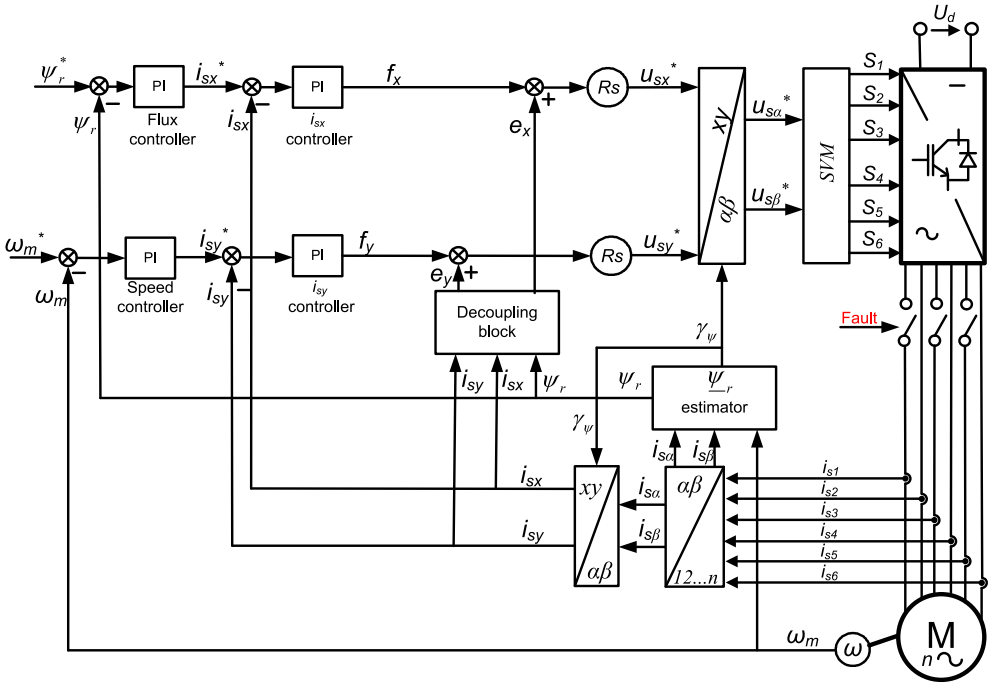

Fig. 5. The control system of six-phase induction motor with Direct Field-Oriented Control

The output control signals from these controllers determine the reference components u^*_{sx} and u^*_{sy} of the stator voltage vector. These values are transformed to the stationary $\alpha-\beta$ coordinate system and given next to the Space Vector Modulator (SVM), which sets the switching states of the multi-phase VSI. In order to improve the dynamical properties of the drive systems, the decoupling blocks have been also applied in the control systems [11].

6. Experimental and simulation results

The first presented results refer to the operating state of the six-phase induction motor with a control lock of a three-phase VSI which forms a six-phase VSI (Fault State 1). These fault state has been analyzed by experimental studies. The experimental research was carried out using the specially designed and built laboratory set-up. The photo of the drive system with a six-phase induction motor with the specification of the system components is shown in Figure 6. The experimental system consists of a six-phase squirrel-cage induction motor with a slip-ring induction motor used as the load machine, a six-phase VSI consisting of two three-phase VSIs, a measuring system with LEM-type sensors and an incremental encoder, a PC computer with Control Desk Software and with the dSpace 1104 Processor card. The control boards that change signals from the processor to the signals transmitted through optical fibers are also applied in the experimental set-up. The three-phase VSIs are able to run independently and this advantage

has been used during the experimental research. The experimental studies were carried out for a 6-phase squirrel-cage induction motor with the following data and parameters: $P_N = 1.5$ kW, $U_{fN} = 230$ V, $f_N = 50$ Hz, $p_b = 2$, $R_s = 7.8\ \Omega$, $R_r = 11\ \Omega$, $L_{ls} = L_{lr} = 0.06$ H, $L_m = 0.75$ H.

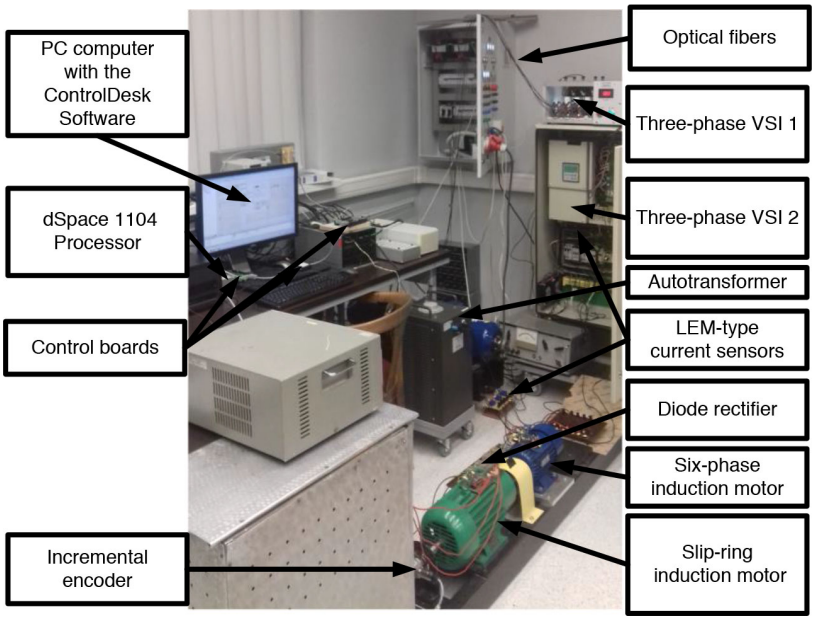

Fig. 6. The photo of the laboratory set-up with six-phase induction motor

The operation of the DFOC with a six-phase induction motor was analyzed for the case of failure, caused by a blocking control signal in the system of one three-phase VSI and the resulting lack of operation of this inverter. It was assumed that this fault condition occurred while the induction motor was running at a constant speed and was previously fed with a symmetrical system of phase voltages. The induction motor was not loaded during this test. The fault state occurred in the time $t = 2.1$ s.

Figure 7 shows the waveforms of the reference and measured mechanical speed of the six-phase induction motor for DFOC control system at Fault State 1.

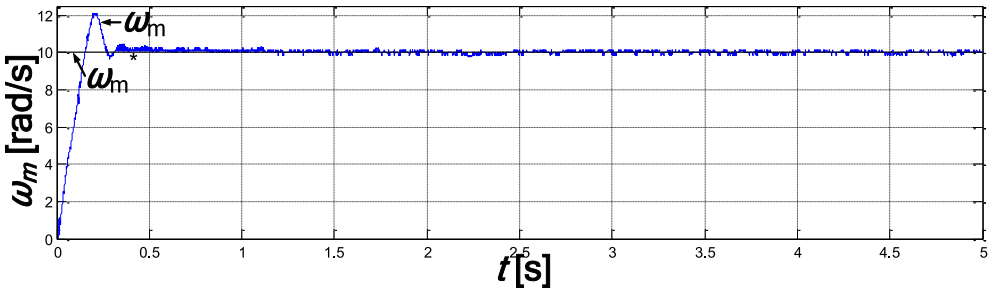

Fig. 7. The experimental waveforms of speeds of the six-phase induction motor for DFOC at Fault State 1

The results of these experimental studies indicate that the occurrence of the considered fault state had no effect on the accuracy of the motor speed control for the analyzed control method. The trajectories of the reference and measured motor speed coincide with high accuracy.

The experimental waveform of the motor electromagnetic torque of the six-phase induction motor for DFOC at Fault State 1 is presented in Figure 8. The analyzed control method ensures proper control of the motor electromagnetic torque during the control system operation at nominal conditions and after the three-phase VSI control lockout.

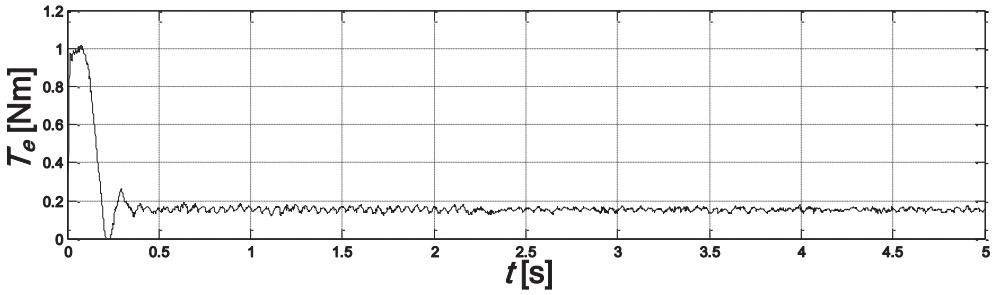

Fig. 8. The experimental waveform of the electromagnetic torque of the six-phase induction motor for DFOC at Fault State 1

The experimental waveforms of the stator phase currents for the DFOC at Fault State 1 have been presented in Figure 9.

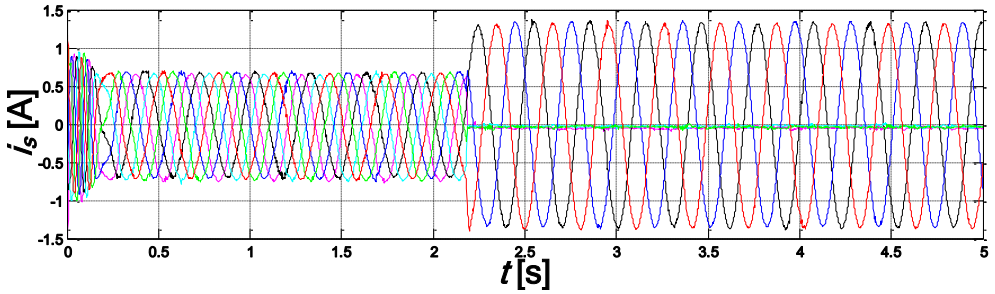

Fig. 9. The experimental waveforms of the stator phase currents of the six-phase induction motor for DFOC at Fault State 1

The time moment of the occurrence of the analyzed fault state is clearly visible in Figure 9. For the analyzed control method after the failure of the control system of the three-phase VSI, the amplitudes of the stator phase currents in the three active phases increased twice, while in the remaining three phases, the phase currents of the six-phase induction motor were zero.

Figure 10 shows the trajectory of the estimated rotor flux vector of the six-phase induction motor for the DFOC at Fault State 1. It can be observed that the rotor flux vector has been regulated correctly at the rated value when the induction motor was powered from an efficient converter system and when the motor is supplied from a single three-phase VSI.

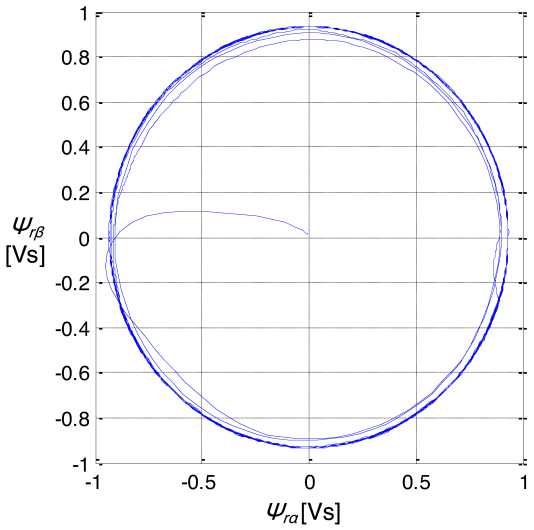

Fig. 10. Trajectory of the estimated rotor flux vector of the six-phase induction motor for DFOC at Fault State 1

Below the analysis of the encoder failure for the DFOC system with a five-phase induction motor has been presented (Fault State 2). The simulation studies have been carried out for the five-phase squirrel-cage induction motor with the parameters: $P_N = 3$ kW, $U_{f_N} = 230$ V, $f_N = 50$ Hz, $p_b = 2$, $R_s = 7.48\ \Omega$, $R_r = 3.68\ \Omega$, $L_{ls} = L_{lr} = 0.0221$ H, $L_m = 0.411$ H. The absence of the measured signal from the encoder was analyzed. The fault state of the encoder has been simulated during the start-up of the five-phase induction motor. The drive system, resistant to the motor speed sensor fault, has been analyzed. After the occurrence of the failure condition of the motor speed sensor, the simulated (considered as measured) speed signal from the speed sensor has been replaced by the estimated speed signal obtained from the MRAS^{CC} estimator.

In Figure 11 the waveforms of the reference speed (black color), simulated speed (blue color) and estimated speed (green color) of the five-phase induction motor for the DFOC at Fault State 2 have been presented.

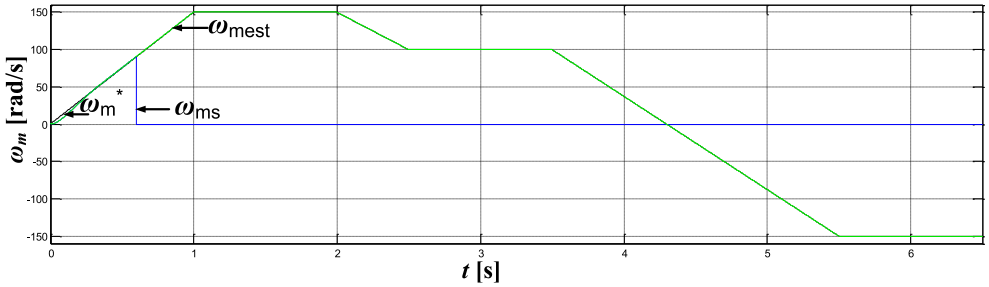

Fig. 11. The simulation waveforms of speeds of the five-phase induction motor for DFOC at Fault State 2

On the basis of the analysis of the presented simulation results, it can be stated that the DFOC system ensures precise control of the five-phase induction motor speed before the failure of the speed sensor. The proper operation is obtained also after the sensor failure, when the control system is switched to sensorless speed control. After the failure of the encoder, the immediate decrease of the motor simulated speed reduced to the zero value occurs. The moment of switching to sensorless speed control is not visible in the waveform of the estimated motor speed.

Figure 12 shows the waveforms of the load torque and the electromagnetic torque of the five-phase induction motor for the DFOC at Fault State 2.

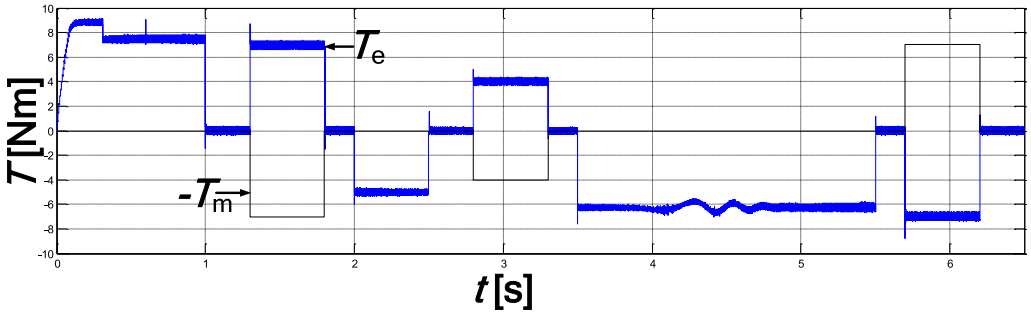

Fig. 12. The simulation waveforms of load torque and electromagnetic torque of the five-phase induction motor for DFOC at Fault State 2

The DFOC control method ensures precise control of the motor electromagnetic torque. The precise regulation of this motor variable occurs when the drive system is working with the measurement of the motor mechanical speed and after the failure of the speed sensor and while working with the estimation of speed by the MRAS^{CC} estimator.

The waveforms of the y component of the stator current vector of the five-phase induction motor for the DFOC at Fault State 2 have been shown in Figure 13.

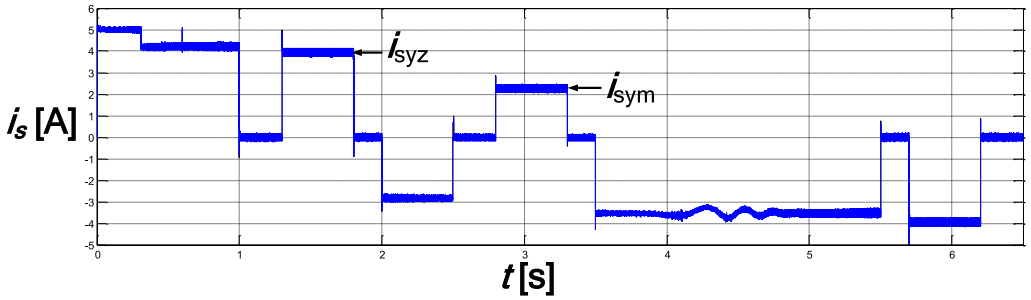

Fig. 13. The simulation waveforms of the y component of the stator current vector of the five-phase induction motor for DFOC at Fault State 2

The considered DFOC method ensures the exact regulation of the analyzed variable of the five-phase induction motor. The exact regulation of this variable of the motor occurs in the same

way as in the electromagnetic torque when the drive system is working with the measurement of the mechanical speed and after the failure of the speed sensor and while working with the estimation of speed by the MRAS^{CC} estimator.

The waveforms of the stator phases currents of the five-phase induction motor have been presented in Figure 14(a) and the waveforms of the reference and estimated magnitude of the rotor flux vector of the five-phase induction motor for the analyzed DFOC control system have been presented in Figure 14(b).

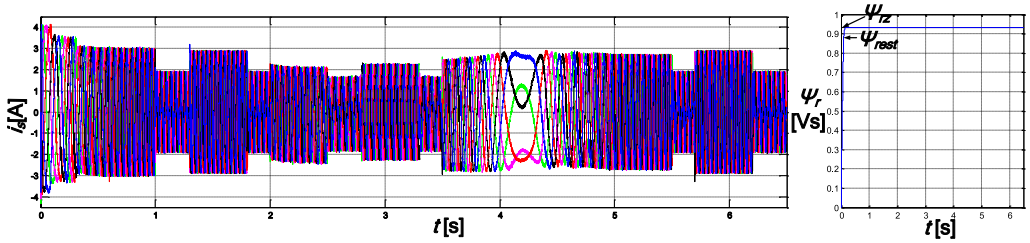

(a) (b)

Fig. 14. The simulation waveforms: (a) the stator phase currents of the five-phase induction motor for DFOC at Fault State 2; (b) the waveforms of the reference and estimated magnitude of the rotor flux vector of the five-phase induction motor for DFOC at Fault State 2

The moment of the motor speed sensor failure and the change of the control system to sensorless speed control are not visible in the stator phase currents. The magnitude of the rotor flux vector is regulated by the control system at the given rated value and the oscillations are not visible during every tested states of the drive system.

7. Conclusions

The mathematical model of a five-phase induction motor, six-phase induction motor, MRAS^{CC} estimator and the Space Vector Modulation have been presented. In the Space Vector Modulation method for five-phase and six-phase VSIs, long and zero voltage vectors have been used. DFOC systems with a five-phase induction motor and with six-phase induction motor have been analyzed.

Two types of faults in drive systems with multi-phase induction motors have been analyzed. Fault State 1, consisting in blocking of the control of a three-phase VSI and Fault State 2 consisting in the damage of the speed sensor, have been chosen to the analysis.

The failure of the power electronics control system did not affect the proper operation of the six-phase induction motor at a given trajectory of the motor speed. According to the simulation results for the DFOC with a five-phase induction motor with fault condition of the speed sensor, it can be stated, that the DFOC control system, resistant to the encoder damage, allowed for precise regulation of the five-phase induction motor variables during the presented states of the drive system.

References

[1] Dujic D., Grandi G., Jones M., Levi E., *A Space Vector PWM Scheme for Multifrequency Output Voltage Generation With Multiphase Voltage-Source Inverters*, IEEE Transactions on Industrial Electronics, vol. 55, iss. 5, pp. 1943–1955 (2008).

[2] Duran M.J., Prieto J., Barrero F., Riveros J.A., Guzman H., *Space-Vector PWM with Reduced Common-Mode Voltage for Five-Phase Induction Motor Drives*, IEEE Transactions on Industrial Electronics, vol. 60, no. 10, pp. 4159–4168 (2013).

[3] Dybkowski M., Klimkowski K., *A Fault Tolerant Control Structure for an Induction Motor Drive System*, Automatika, vol. 57, no. 3, pp. 638–647 (2016).

[4] Dybkowski M., Klimkowski K., Orlowska-Kowalska T., *Speed and Current Sensor Fault-Tolerant Control of the Induction Motor Drive*, Advanced Control of Electrical Drives and Power Electronic Converters, Springer, pp. 141–167 (2017).

[5] Kianinezhad R., Nahid B., Betin F., Capolino G., *Multi-Vector SVM: A New Approach to Space Vector Modulation Control for Six-Phase Induction Machines*, Proceedings of IECON, pp. 1359−1364, 6–10 November (2005).

[6] Levi E., Bojoi R., Profumo F., Toliyat H.A., Williamson S., *Multiphase Induction Motor Drives – a Technology Status Review*, IET Electric Power Applications, vol. 1, iss. 4, pp. 489–516 (2007).

[7] Levi E., Satiavan I., Bodo N., Jones M., *A Space-Vector Modulation Scheme for Multilevel Open-End Winding Five-Phase Drives*, IEEE Transactions on Energy Conversion, vol. 27, iss. 1, pp. 1−10 (2012).

[8] Listwan J., Pienkowski K., *Field-Oriented Control of Five-Phase Induction Motor with Open-End Stator Winding*, Archives of Electrical Engineering, vol. 65, no 3, pp. 395–410 (2016).

[9] Listwan J., Pienkowski K., *DTC-ST and DTC-SVM Control of Five-Phase Induction Motor with MRAS^{CC} Estimator*, Przegląd Elektrotechniczny, vol. 92, no. 11, pp. 252–256 (2016).

[10] Lu S., Corzine K., *Direct Torque Control of Five-Phase Induction Motor Using Space Vector Modulation with Harmonics Elimination and Optimal Switching Sequence*, Twenty-First Annual IEEE Applied Power Electronics Conference and Exposition (APEC), Dallas, USA, pp. 195−201, 19–23 March (2006).

[11] Orlowska-Kowalska T., *Sensorless Induction Motor Drives*, Oficyna Wydawnicza Politechniki Wrocławskiej (in Polish) (2003).

[12] Pienkowski K., *Analysis and control of the multiphase squirrel-cage induction motor*, Prace Naukowe Instytutu Maszyn, Napędów i Pomiarów Elektrycznych Politechniki Wrocławskiej (in Polish), no. 65, pp. 305–319 (2011)

[13] Rolak M., Malinowski M., *Six-Phase Symmetrical Induction Machine Under Fault States – Modelling*, Simulation and Experimental Results, Przegląd Elektrotechniczny, vol. 90, no. 11, pp. 91–95 (2014).

[14] Tani A., Mengoni M., Zarri L., Serra G., Casadei D., *Control of Multiphase Induction Motors with an Odd Number of Phases Under Open-Circuit Phase Faults*, IEEE Transactions on Power Electronics, vol. 27, no. 2, pp. 565–577 (2012).